



Melting heat and viscous dissipation in flow of hybrid nanomaterial: a numerical study via finite difference method

T. Hayat^{1,2} · Khursheed Muhammad¹ · S. Momani^{3,4}

Received: 1 March 2021 / Accepted: 7 June 2021 / Published online: 11 July 2021
© Akadémiai Kiadó, Budapest, Hungary 2021

Abstract

Hybrid nanomaterial flowing through Darcy–Forchheimer (D–C) porous medium bounded between two infinite parallel walls is considered in this analysis. The lower wall is fixed and stretchable, while the upper wall moves (squeezes) toward lower one. Cattaneo–Christov (C–C) heat flux is addressed instead of traditional Fourier’s heat flux. Further lower wall is subjected to melting heat. Viscous dissipation accounts heat transport features. Hybrid nanomaterial is constructed through dispersion of both GO (Grapheneoxide) and Cu (Copper) nanoparticles in the water-based liquid. Mathematical formulation in form of PDEs is done. Resulting PDEs are then non-dimensionalized via choosing suitable variables. Numerical technique namely FDM (finite difference method) through FD (forward difference) approximations is executed for these PDEs in order to construct the solutions. Moreover, the velocities and temperature are expressed graphically through involved physical parameters. Velocity of hybrid nanofluid (GO + Cu + Water) enhances with higher estimations of squeezing parameter and Reynolds number while it reduces with an increment in Forchheimer number and porosity parameter. Reduction in temperature of hybrid nanofluid (GO + Cu + Water) is noticed against larger melting parameter while it boosts for higher squeezing parameter and Eckert number.

Keywords Melting heat · Cattaneo–Christov (C–C) heat flux · Viscous dissipation · FDM · Hybrid nanomaterial (GO + Cu + Water) · Darcy–Forchheimer (D–F) porous medium · Squeezing flow

Introduction

In order to overcome rise in the energy requirements due to advancement in technological and industrial processes, the only way is to use renewable energy. That is why the scientists and researchers are devoted toward developing devices with advanced rate of cooling or heat which results in saving and storing of energy. The most appropriate, rich and easy source of such energy (renewable energy) is the solar energy. For this purpose thermal solar collectors are constructed in

which ordinary fluids are used as heat transport medium. Such ordinary fluids possess very small thermal conductance and heat storing capacity due to which the performance of solar collectors is affected. Facing such issue, investigators focused toward developing materials possessing higher thermal conductance and thermal storing capacity. In this regard, pioneer work is done by Choi et al. [1, 2]. They observed better thermal conductance of the material obtained by adding nano-sized (1–100 nm) particles in the ordinary fluids. Such material is called nanofluid and the added nano-sized substances are called nanoparticles. A basic review work on hybrid nanomaterial is presented by Sarkar et al. [3]. Melting heat with chemical reactions in CNTs-nanomaterial is elaborated by Hayat et al. [4]. Hosseini et al. [5] examined entropy and MHD effects for nanomaterials flow with heat generation. Some latest investigations regarding nanomaterials flows are given in Refs. [6–28].

Although heat transport process is recently the core area of study but little interest has been shown toward studying heat transport via melting process. Melting heat plays a vital role in engineering, physics, technological and industrial processes.

✉ Khursheed Muhammad
kmuhammad@math.qau.edu.pk; khursheedfaiq@gmail.com

¹ Department of Mathematics, Quaid-I-Azam University, Islamabad 44000, Pakistan

² Pakistan Academy of Sciences (PAS), G-5/2, Islamabad, Pakistan

³ Nonlinear Dynamics Research Centre (NRDC), Ajman University, Ajman, UAE

⁴ Department of Mathematics, Faculty of Science, University of Jordan, Amman 11942, Jordan

Due to applications in aforementioned fields, investigators and researchers have shown great devotion toward developing effective and sustainable technologies for energy storage. The process of storing energy involves latent heat, sensible heat and chemical heat mechanisms. Among these mechanisms, latent heat is the most efficient and economically friendly for storing energy. Melting process is directly related to the latent heat. Melting condition stores the energy in the material while this stored energy can be regained through freezing. Manufacturing of semi-conductors, soil melting, magma solidification, permafrost melting, freezing treatment of sewage, frozen ground thawing and many more are the applications of melting phenomenon. Initial analysis on melting heat by placing ice slab in stream of hot air is performed by Rebert et al. [29]. Chemical reactions, melting and MHD impacts on tangent hyperbolic material flow due to nonlinear stretching surface is expressed by Qayyum et al. [30]. Qi et al. [31] studied heat transmission during melting process of lauric acid in a cavity. Few updated analyses on melting heat can be seen in Refs. [32–39].

Literature shows that researchers have shown their attentions toward studying nanomaterials. Hybrid nanomaterials are discussed rare up to date. Further this analysis narrowed down when squeezing flow is considered in presence of Cattaneo–Christov (C–C) heat flux and Darcy–Forchheimer (D-F) porous medium. Thus, to fill up this void the hybrid nanomaterial (GO + Cu + Water) flow through Darcy–Forchheimer (D-F) porous medium bounded between two parallel walls is examined in this analysis. Lower stretching wall is subject to melting. Cattaneo–Christov (C–C) heat flux is addressed. Viscous dissipation is accounted. Related expressions of PDEs are constructed and then non-dimensionalized

through suitable variables. Such non-dimensional PDEs are then solved by finite difference method. Velocities and temperature are examined under involved parameters graphically.

Mathematical modeling

Consider 2D unsteady flow of hybrid nanomaterial confined between two infinite walls. The lower wall $y = 0$ is fixed and stretches with velocity $U_w(x, t)$, while upper wall $y = h(t)$ moves (squeezes) toward lower wall with velocity $V_h(t)$. Both the walls are at a distance $h(t)$ from each other. Darcy–Forchheimer (D–C) porous medium is taken between these walls and hybrid nanomaterial flow through it. Disturbance in hybrid nanomaterial is generated by stretching the lower wall. Lower wall is also subjected to melting heat effect and Cattaneo–Christov (C–C) heat flux instead of ordinary Fourier’s heat flux (see Fig. 1). Hybrid nanomaterial is made by adding two types of nanoparticles (GO, Cu) in water-based fluid.

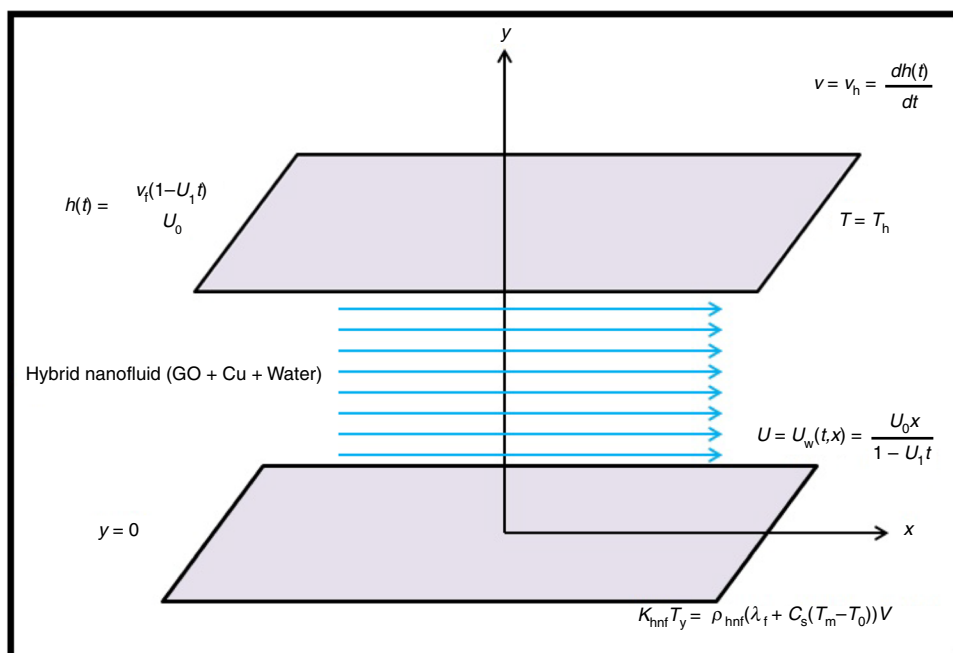
Making use of above-mentioned assumptions, the flow and heat related expressions (PDEs) are [7]:

$$U_x + V_y = 0, \tag{1}$$

$$U_t + UU_x + VU_y = \nu_{hnf}(U_{xx} + U_{yy}) - \frac{\nu_{hnf}}{k_1}\phi_0 U - \frac{c_b}{\sqrt{k_1}}U^2, \tag{2}$$

$$V_t + UV_x + VU_y = \nu_{hnf}(U_{xx} + V_{yy}) - \frac{\nu_{hnf}}{k_1}\phi_0 V - \frac{c_b}{\sqrt{k_1}}V^2, \tag{3}$$

Fig. 1 Physical diagram for considered problem



$$\begin{aligned}
 T_t + UT_x + VT_y + \tau_0[T_{tt} + UU_xT_x + VV_yT_y + UV_xT_y + VU_yT_x \\
 + 2UVT_{xy} + U^2T_{xx} + V^2T_{yy} + U_tT_x + 2UT_{xt} + V_tT_y + 2VT_{ty}] \\
 = \alpha_{\text{hnf}}[T_{xx} + T_{yy}] + \frac{\mu_{\text{hnf}}}{(\rho c_p)_{\text{hnf}}}(4(U_x)^2 + (V_x + U_y)^2),
 \end{aligned}
 \tag{4}$$

with IBCs (initial and boundary conditions)

$$\begin{aligned}
 U = 0, \quad V = 0, \quad T = T_w, \quad T_t = 0 \quad \text{when } t = 0 \\
 U = U_w(t, x) = \frac{U_0x}{1 - U_1t}, \quad T = T_m, \\
 k_{\text{hnf}}T_y = \rho_{\text{hnf}}(\lambda_f + C_s(T_m - T_0))V \quad \text{when } y = 0, \\
 U = 0, \quad V = V_h(t) = h(t)t, \quad T = T_h \quad \text{when } y = h(t).
 \end{aligned}
 \tag{5}$$

In above equations U, V and T are functions of x, y and t while $h(t) = \sqrt{\frac{v_f(1-U_1t)}{U_0}}$.

Consider the dimensionless quantities

$$\begin{aligned}
 f = \frac{L}{v_f}U, \quad g = \frac{L}{v_f}V, \quad t^* = \frac{v_f}{L^2}t, \quad y^* = \frac{y}{L}, \quad x^* = \frac{x}{L}, \\
 \theta = \frac{T - T_m}{T_h - T_m}, \quad \text{Pr} = \frac{v_f}{\alpha_f}, \quad \text{Sq} = \frac{U_1}{U_0}, \quad \lambda = \frac{L^2\phi_0}{\sqrt{k_1}}, \\
 \gamma = \frac{\tau_0 v_f}{L^2}, \quad M = \frac{U_0 L^2}{v_f - U_1 t^* L^2}, \quad M_1 = \frac{(T_h - T_m)(c_p)_f}{\lambda_f + C_s(T_m - T_0)}, \\
 \text{Fr} = \frac{c_b L}{\sqrt{k_1}}, \quad \text{Ec} = \frac{\mu_f \alpha_f}{L^2(\rho c_p)(T_h - T_m)}.
 \end{aligned}
 \tag{6}$$

Using these variables in Eqs. (1–5), we are left with the following dimensionless DEs and IBCs

$$f_{x^*} + g_{y^*} = 0, \tag{7}$$

$$f_{t^*} + ff_{x^*} + gf_{y^*} = A_{11}(f_{x^*x^*} - \lambda f + f_{y^*y^*}) - \text{Fr}(f)^2, \tag{8}$$

$$g_{t^*} + fg_{x^*} + gg_{y^*} = A_{11}(g_{x^*x^*} - \lambda g + g_{y^*y^*}) - \text{Fr}(g)^2, \tag{9}$$

$$\begin{aligned}
 \theta_{t^*} + f\theta_{x^*} + g\theta_{y^*} + \gamma[\theta_{t^*t^*} + f(t^*, x^*, y^*)f_{x^*}\theta_{x^*} \\
 + gg_{y^*}\theta_{y^*} + fg_{x^*}\theta_{y^*} + vf_{y^*}\theta_{x^*} + 2fg\theta_{x^*y^*} + f^2\theta_{x^*x^*} \\
 + g^2\theta_{y^*y^*} + 2fg\theta_{x^*y^*} + f^2\theta_{x^*x^*} + g^2\theta_{y^*y^*} + f_{t^*}\theta_{x^*} \\
 + 2f\theta_{x^*t^*} + g_{t^*}\theta_{y^*} + 2g\theta_{t^*y^*}] = \frac{A_{16}}{A_{21}} \text{Pr Ec}(4(f_{x^*})^2 \\
 + (g_{x^*} + f_{y^*})^2) + \frac{A_{14}}{A_{15} \text{Pr}}[\theta_{x^*x^*} + \theta_{y^*y^*}].
 \end{aligned}
 \tag{10}$$

Dimensionless IBCs are

$$\begin{aligned}
 f = 0, \quad g = 0, \quad \theta = 1, \quad \theta_{t^*} = 0 \quad \text{when } t^* = 0, \\
 f = Mx^*, \quad \theta = 1, \quad g = 0, \quad \frac{M_1}{A_{14}}\theta_{y^*} = \frac{\text{Pr}}{A_{21}}g \quad \text{when } y^* = 0, \\
 f = 0, \quad g = \frac{\text{Sq}}{2}\sqrt{M}, \quad \theta = 0 \quad \text{when } y^* = 1.
 \end{aligned}
 \tag{11}$$

Here

$$\begin{aligned}
 A_{11} &= \frac{v_{\text{hnf}}}{v_f} \\
 &= \frac{1}{(1 - \phi_1)^{2.5}(1 - \phi_2)^{2.5}[(1 - \phi_2)\left((1 - \phi_1) + \phi_1 \frac{\rho_{s1}}{\rho_f}\right) + \phi_2 \frac{\rho_{s2}}{\rho_f}]}
 \end{aligned}
 \tag{12}$$

$$A_{14} = \frac{k_{\text{hnf}}}{k_f}, \tag{13}$$

$$A_{15} = \left((1 - \phi_2) \left((1 - \phi_1) + \phi_1 \frac{(\rho c_p)_{s1}}{(\rho c_p)_f} \right) + \phi_2 \frac{(\rho c_p)_{s2}}{(\rho c_p)_f} \right), \tag{14}$$

$$A_{16} = \frac{1}{(1 - \phi_1)^{2.5}(1 - \phi_2)^{2.5}}. \tag{15}$$

$$A_{21} = \frac{\rho_{\text{hnf}}}{\rho_f}. \tag{16}$$

In above relations f, g and θ are functions of t^*, x^* and y^* .

Hybrid nanomaterial (GO + Cu + Water) expressions via Hamilton–Crosser model

Expressions for hybrid nanomaterial (GO + Cu + Water) proposed by Hamilton–Crosser model are [7]

$$\mu_{\text{hnf}} = \frac{\mu_f}{(1 - \phi_1)^{2.5}(1 - \phi_2)^{2.5}}, \quad \nu_{\text{hnf}} = \frac{\mu_{\text{hnf}}}{\rho_{\text{hnf}}}, \tag{17}$$

$$(\rho c_p)_{\text{hnf}} = (1 - \phi_2) \left((1 - \phi_1)(\rho c_p)_f + \phi_1(\rho c_p)_{s1} \right) + \phi_2(\rho c_p)_{s2}, \tag{18}$$

$$\rho_{\text{hnf}} = (1 - \phi_2) \left((1 - \phi_1) \rho_f + \phi_1 \rho_{s1} \right) + \phi_2 \rho_{s2}, \tag{19}$$

$$\frac{\kappa_{\text{hnf}}}{\kappa_{\text{nf}}} = \frac{\kappa_{s2} + (n - 1)\kappa_{\text{nf}} - (n - 1)\phi_2(\kappa_{\text{nf}} - \kappa_{s2})}{\kappa_{s2} + (n - 1)\kappa_{\text{nf}} + \phi_2(\kappa_{\text{nf}} - \kappa_{s2})} \tag{20}$$

Here n represents shape of nanoparticles (GO, Cu). We have chosen $n = 6$ as we are interested in tube like or cylindrical nanoparticles.

Solutions methodology

The obtained relevant expressions (PDEs) of the problem are non-dimensionalized by choosing appropriate dimensionless variables. These PDEs are then solved numerically via FDM. This methodology is implemented on FDEs (finite difference equations). Thus, we have converted our dimensionless PDEs and IBCs into FDEs using FD forward difference approximations as below [39–43].

$$\begin{aligned}
 f_{t^*} &= \frac{f_{ij}^{n+1} - f_{ij}^n}{h_n}, \quad f_{x^*} = \frac{f_{i+1,j}^n - f_{ij}^n}{h_i}, \\
 f_{y^*} &= \frac{f_{i,j+1}^n - f_{ij}^n}{h_j}, \quad g_{t^*} = \frac{g_{ij}^{n+1} - g_{ij}^n}{h_n}, \\
 g_{x^*} &= \frac{g_{i+1,j}^n - g_{ij}^n}{h_i}, \quad g_{y^*} = \frac{g_{i,j+1}^n - g_{ij}^n}{h_j}, \\
 \theta_{t^*} &= \frac{\theta_{ij}^{n+1} - \theta_{ij}^n}{h_n}, \quad \theta_{x^*} = \frac{\theta_{i+1,j}^n - \theta_{ij}^n}{h_i}, \\
 \theta_{y^*} &= \frac{\theta_{i,j+1}^n - \theta_{ij}^n}{h_j}.
 \end{aligned}
 \tag{21}$$

$$\begin{aligned}
 f_{x^*x^*} &= \frac{f_{i+2,j}^n - 2f_{i+1,j}^n + f_{ij}^n}{h_i^2}, \quad f_{y^*y^*} = \frac{f_{i,j+2}^n - 2f_{i,j+1}^n + f_{ij}^n}{h_j^2}, \\
 g_{x^*x^*} &= \frac{g_{i+2,j}^n - 2g_{i+1,j}^n + g_{ij}^n}{h_i^2}, \quad g_{y^*y^*} = \frac{g_{i,j+2}^n - 2g_{i,j+1}^n + g_{ij}^n}{h_j^2}, \\
 \theta_{t^*t^*} &= \frac{\theta_{ij}^{n+2} - 2\theta_{ij}^{n+1} + \theta_{ij}^n}{h_j^2}, \quad \theta_{x^*x^*} = \frac{\theta_{i+2,j}^n - 2\theta_{i+1,j}^n + \theta_{ij}^n}{h_i^2}, \\
 \theta_{y^*y^*} &= \frac{\theta_{i,j+2}^n - 2\theta_{i,j+1}^n + \theta_{ij}^n}{h_j^2}, \quad f_{x^*r^*} = \frac{f_{i+1,j}^{n+1} - f_{i+1,j}^n - f_{ij}^{n+1} + f_{ij}^n}{h_i h_n}, \\
 f_{y^*r^*} &= \frac{f_{i,j+1}^{n+1} - f_{i,j+1}^n - f_{ij}^{n+1} + f_{ij}^n}{h_j h_n}, \quad f_{x^*y^*} = \frac{f_{i+1,j+1}^n - f_{i+1,j}^n - f_{i,j+1}^n + f_{ij}^n}{h_i h_j}, \\
 g_{x^*r^*} &= \frac{g_{i+1,j}^{n+1} - g_{i+1,j}^n - g_{ij}^{n+1} + g_{ij}^n}{h_i h_n}, \quad g_{y^*r^*} = \frac{g_{i,j+1}^{n+1} - g_{i,j+1}^n - g_{ij}^{n+1} + g_{ij}^n}{h_j h_n}, \\
 g_{x^*y^*} &= \frac{g_{i+1,j+1}^n - g_{i+1,j}^n - g_{i,j+1}^n + g_{ij}^n}{h_i h_j}, \quad \theta_{x^*r^*} = \frac{\theta_{i+1,j}^{n+1} - \theta_{i+1,j}^n - \theta_{ij}^{n+1} + \theta_{ij}^n}{h_i h_n}, \\
 \theta_{y^*r^*} &= \frac{\theta_{i,j+1}^{n+1} - \theta_{i,j+1}^n - \theta_{ij}^{n+1} + \theta_{ij}^n}{h_j h_n}, \quad \theta_{x^*y^*} = \frac{\theta_{i+1,j+1}^n - \theta_{i+1,j}^n - \theta_{i,j+1}^n + \theta_{ij}^n}{h_i h_j}.
 \end{aligned}
 \tag{22}$$

Using these approximations in Eqs. (8)-(11), we get

$$\frac{f_{i+1,j}^n - f_{ij}^n}{h_i} + \frac{g_{i,j+1}^n - g_{ij}^n}{h_j} = 0,
 \tag{23}$$

$$\begin{aligned}
 &\frac{f_{ij}^{n+1} - f_{ij}^n}{h_n} + f_{ij}^n \left[\frac{f_{i+1,j}^n - f_{ij}^n}{h_i} + g_{ij}^n \frac{f_{i,j+1}^n - f_{ij}^n}{h_j} \right. \\
 &= -\text{Fr}(f_{ij}^n)^2 + A_{11} \left[\frac{f_{i+2,j}^n - 2f_{i+1,j}^n + f_{ij}^n}{h_i^2} \right. \\
 &\quad \left. - \lambda f_{ij}^n + \frac{f_{i,j+2}^n - 2f_{i,j+1}^n + f_{ij}^n}{h_j^2} \right],
 \end{aligned}
 \tag{24}$$

$$\begin{aligned}
 &\frac{g_{ij}^{n+1} - g_{ij}^n}{h_n} + f_{ij}^n \frac{g_{i+1,j}^n - g_{ij}^n}{h_i} + g_{ij}^n \frac{g_{i,j+1}^n - g_{ij}^n}{h_j} \\
 &= -\text{Fr}(g_{ij}^n)^2 + A_{11} \left[\frac{g_{i+2,j}^n - 2g_{i+1,j}^n + g_{ij}^n}{h_i^2} \right. \\
 &\quad \left. - \lambda g_{ij}^n + \frac{g_{i,j+2}^n - 2g_{i,j+1}^n + g_{ij}^n}{h_j^2} \right],
 \end{aligned}
 \tag{25}$$

$$\begin{aligned}
 &\frac{\theta_{ij}^{n+1} - \theta_{ij}^n}{h_n} + f_{ij}^n \frac{\theta_{i+1,j}^n - \theta_{ij}^n}{h_i} + g_{ij}^n \frac{\theta_{i,j+1}^n - \theta_{ij}^n}{h_j} \\
 &+ \gamma \left[\frac{\theta_{ij}^{n+2} - 2\theta_{ij}^{n+1} + \theta_{ij}^n}{h_j^2} + i_j^n \frac{f_{i+1,j}^n - f_{ij}^n}{h_i} \frac{\theta_{i+1,j}^n - \theta_{ij}^n}{h_i} \right. \\
 &+ g_{ij}^n \frac{g_{i+1,j}^n - g_{ij}^n}{h_j} \frac{\theta_{i+1,j}^n - \theta_{ij}^n}{h_j} + f_{ij}^n \frac{g_{i+1,j}^n - g_{ij}^n}{h_i} \frac{\theta_{i+1,j}^n - \theta_{ij}^n}{h_j} \\
 &+ g_{ij}^n \frac{f_{i+1,j}^n - f_{ij}^n}{h_j} \frac{\theta_{i+1,j}^n - \theta_{ij}^n}{h_i} \\
 &+ 2f_{ij}^n g_{ij}^n \frac{g_{i+1,j+1}^n(t^*, x^*, y^*) - g_{i+1,j}^n - g_{i,j+1}^n + g_{ij}^n}{h_i h_j} \\
 &+ f_{ij}^n \frac{\theta_{i+2,j}^n - 2\theta_{i+1,j}^n + \theta_{ij}^n}{h_i^2} \\
 &+ g_{ij}^n \frac{\theta_{i,j+2}^n - 2\theta_{i,j+1}^n + \theta_{ij}^n}{h_j^2}
 \end{aligned}
 \tag{26}$$

$$\begin{aligned}
 &+ \frac{f_{ij}^{n+1} - f_{ij}^n}{h_n} \frac{\theta_{i+1,j}^n - \theta_{ij}^n}{h_i} \\
 &+ 2f_{ij}^n \frac{\theta_{i+1,j}^{n+1} - \theta_{i+1,j}^n - \theta_{ij}^{n+1} + \theta_{ij}^n}{h_i h_n} \\
 &+ \frac{g_{ij}^{n+1} - g_{ij}^n}{h_n} \frac{\theta_{i+1,j}^n - \theta_{ij}^n}{h_j} 2g_{ij}^n \frac{\theta_{i+1,j}^{n+1} - \theta_{i+1,j}^n - \theta_{ij}^{n+1} + \theta_{ij}^n}{h_i h_n} \\
 &= \frac{A_{16}}{A_{21}} \text{Pr Ec} \left(4 \left(\frac{f_{i+1,j}^n - f_{ij}^n}{h_i} \right)^2 + \left(\frac{g_{i+1,j}^n - g_{ij}^n}{h_i} + \frac{f_{i,j+1}^n - f_{ij}^n}{h_j} \right)^2 \right) \\
 &+ \frac{A_{14}}{A_{15}} \text{Pr} \left[\frac{\theta_{i+2,j}^n - 2\theta_{i+1,j}^n + \theta_{ij}^n}{h_i^2} + \frac{\theta_{i,j+2}^n - 2\theta_{i,j+1}^n + \theta_{ij}^n}{h_j^2} \right],
 \end{aligned}$$

with IBCs

$$f_{ij}^0 = 0, \quad g_{ij}^0 = 0, \quad \theta_{ij}^0 = 1, \quad \frac{\theta_{ij}^1 - \theta_{ij}^0}{h_0} = 0,
 \tag{27}$$

$$\begin{aligned}
 f_{i,0}^n &= M(x_{i+1}^* - x_i^*), \\
 \theta_{i,0}^n &= 1, \quad \frac{M_1}{A_{14}} \frac{\theta_{i,1}^n - \theta_{i,0}^n}{h_0} \\
 &= \frac{\text{Pr}}{A_{21}} g_{i,0}^n f_{i,1}^n = 0, \\
 g_{i,1}^n &= \frac{Sq}{2} \sqrt{M}, \quad \theta_{i,1}^n = 0.
 \end{aligned}
 \tag{28}$$

Discussion

Impacts of concerned physical variables toward velocities ($f(t^*, x^*, y^*)$, $g(t^*, x^*, y^*)$) and temperature ($\theta(t^*, x^*, y^*)$) are enclosed in this section. Involved parameters and expressions are listed in nomenclature (see Table 1). Table 2 comprises thermal features of nanoparticles (GO, Cu) and baseliquid (water). During analyzing impacts of concerned parameters toward $f(t^*, x^*, y^*)$, $g(t^*, x^*, y^*)$ and $\theta(t^*, x^*, y^*)$, $t^* = 1.0$ and $x^* = 0.1$ for line graphs while in Hamilton–Crosser expressions for hybrid nanomaterial (GO + Cu + Water), $n = 6$ is taken for cylindrical nanoparticles.

Table 1 Nomenclature

| Expression | SI unit | Name | Expression | SI unit | Name |
|--|-------------------------|----------------------------------|--------------------------------------|-------------------------|-------------------------------------|
| u, v | $m\ s^{-1}$ | Components of velocity | $(c_p)_f$ | $m^2\ s^{-2}\ K^{-1}$ | Specific heat of basefluid |
| x, y | M | Cartesian coordinates | Pr | Dimensionless | Prandtl number |
| μ_f | $kg\ m^{-1}\ s^{-1}$ | Fluid dynamic viscosity | τ_w | N m (Pa) | Wall shear stress |
| ν_f | $m^2\ s^{-1}$ | Kinematic fluid viscosity | U_w, V_h | $m\ s^{-1}$ | Stretching and squeezing velocities |
| ρ_f | $kg\ m^{-3}$ | Density of basefluid | GO | | Graphene oxide |
| k_f | $kg\ m\ K^{-1}\ s^{-3}$ | Fluid thermal conductivity | $U_w(t, x)$ | $m\ s^{-1}$ | Stretching surface velocity |
| α_f | $m^2\ s^{-1}$ | Thermal diffusivity of basefluid | M | Dimensionless | Reynolds number |
| $f(t^*, x^*, y^*), g(t^*, x^*, y^*)$ | Dimensionless | Non-dimensional velocities | T_w | K^{-1} | Temperature of lower wall |
| $\theta(t^*, x^*, y^*)$ | Dimensionless | Non-dimensional temperature | k_{s_1} | $kg\ m\ K^{-1}\ s^{-3}$ | Thermal conductivity of GO |
| Cu | | Copper | k_{s_2} | $kg\ m\ K^{-1}\ s^{-3}$ | Thermal conductivity of Cu |
| ϕ_0 | Dimensionless | Porosity of porous medium | ϕ_2 | Dimensionless | Cu volume fraction |
| k_1 | m^2 | Permeability of porous medium | ϕ_1 | Dimensionless | GO volume fraction |
| Sq | Dimensionless | Squeezing parameter | U_0, U_1 | s^{-1} | Arbitrary constants |
| t^*, x^*, y^* | Dimensionless | Dimensionless variables | T_h | K^{-1} | Upper surface temperature |
| γ | Dimensionless | Relaxation time parameter | τ_0 | s | Thermal relaxation time coefficient |
| λ | Dimensionless | Porosity parameter | Fr | Dimensionless | Forchheimer number |
| M_1 | Dimensionless | Melting parameter | Ec | Dimensionless | Eckert number |
| <i>Hybrid Nanofluid (GO + Ag + Kerosene oil)</i> | | | <i>Nanofluid (GO + Kerosene Oil)</i> | | |
| μ_{hnf} | $kg\ m^{-1}\ s^{-1}$ | Dynamic viscosity | k_{nf} | $kg\ m\ K^{-1}\ s^{-3}$ | Thermal conductivity |
| ν_{hnf} | $m^2\ s^{-1}$ | Kinematic viscosity | α_{nf} | $m^2\ s^{-1}$ | Thermal diffusivity |
| ρ_{hnf} | $kg\ m^{-3}$ | Density | $(c_p)_{nf}$ | $m^2\ s^{-2}\ K^{-1}$ | Specific heat |
| k_{hnf} | $kg\ m\ K^{-1}\ s^{-3}$ | Thermal conductivity | μ_{nf} | $kg\ m^{-1}\ s^{-1}$ | Dynamic viscosity |
| α_{hnf} | $m^2\ s^{-1}$ | Thermal diffusivity | ν_{nf} | $m^2\ s^{-1}$ | Kinematic viscosity |
| $(c_p)_{hnf}$ | $m^2\ s^{-2}\ K^{-1}$ | Specific heat | ρ_{nf} | $kg\ m^{-3}$ | Density |

Table 2 Features of nanoparticles (GO, Cu) and basefluid (water) [7, 25]

| Substance\ characteristics | $\rho/kg\ m^{-3}$ | $\kappa/W\ m^{-1}\ K^{-1}$ | $c_p/J\ kg^{-1}\ K^{-1}$ | Pr |
|----------------------------|-------------------|----------------------------|--------------------------|-----|
| Water | 997.1 | 0.613 | 4179 | 6.2 |
| GO | 1880 | s | 717 | – |
| Cu | 632 | 76.5 | 531.8 | – |

Discussion for $f(t^*, x^*, y^*)$ and $g(t^*, x^*, y^*)$

Velocity ($f(t^*, x^*, y^*)$) of hybrid nanomaterial (GO + Cu + Water) due to an increase in Sq (squeezing parameter) is captured in Fig. 2. This figure elaborates that $f(t^*, x^*, y^*)$ increases with higher Sq (squeezing parameter). Physically an increase in Sq (squeezing parameter) is related with execution of more squeezing force from upper wall on the hybrid nanomaterial (GO + Cu + Water) confined between the walls. Due to this squeezing force the velocity ($f(t^*, x^*, y^*)$) of the hybrid nanomaterial (GO + Cu + Water) increases. Figure 3 is made for studying

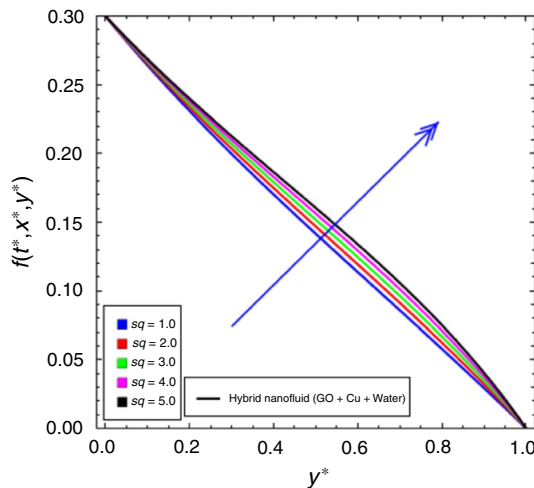


Fig. 2 Velocity ($f(t^*, x^*, y^*)$) against higher Sq

impact of λ (porosity parameter) on velocity ($f(t^*, x^*, y^*)$) of the hybrid nanomaterial (GO + Cu + Water). This figure shows that velocity ($f(t^*, x^*, y^*)$) reduces with higher λ (porosity parameter). Reason behind this reduction in

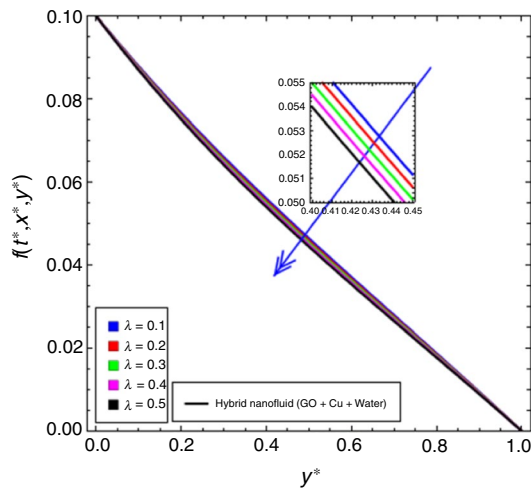


Fig. 3 Velocity ($f(t^*, x^*, y^*)$) against higher λ

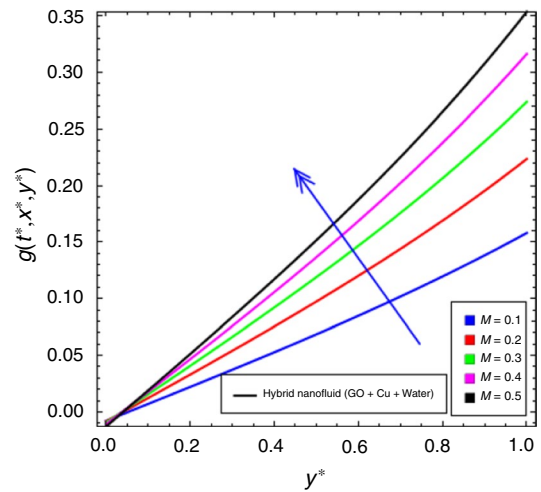


Fig. 6 Velocity ($g(t^*, x^*, y^*)$) against higher M

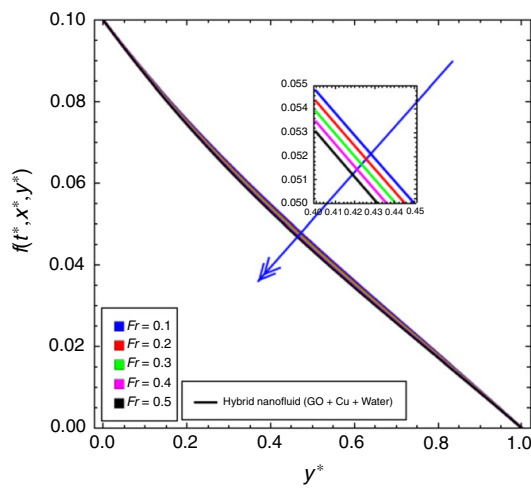


Fig. 4 Velocity ($f(t^*, x^*, y^*)$) against higher Fr

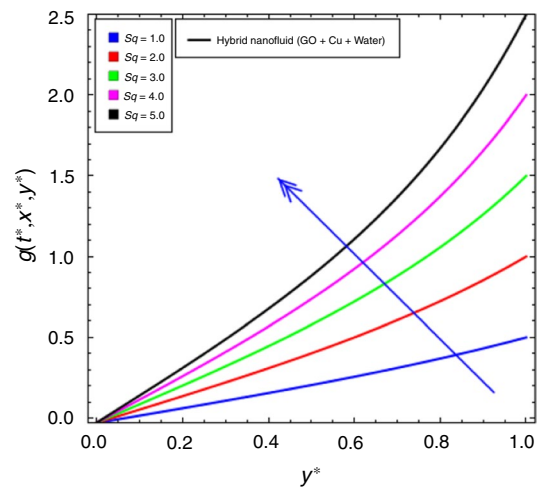


Fig. 7 Velocity ($g(t^*, x^*, y^*)$) against higher Sq

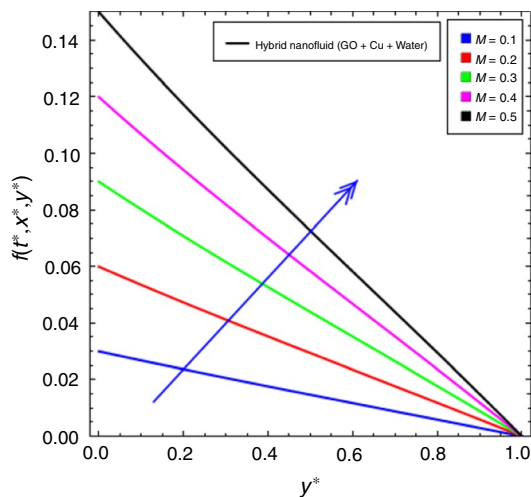


Fig. 5 Velocity ($f(t^*, x^*, y^*)$) against higher M

$f(t^*, x^*, y^*)$ is that higher λ (porosity parameter) relate with production of more porous space among hybrid nanomaterial (GO + Cu + Water). Such porous space resists flow of hybrid nanomaterial (GO + Cu + Water) and correspondingly $f(t^*, x^*, y^*)$ reduces. Velocity ($f(t^*, x^*, y^*)$) of hybrid nanomaterial (GO + Cu + Water) against variations in Fr (Forchheimer number) is expressed in Fig. 4. This plot reveals that $f(t^*, x^*, y^*)$ is a decreasing function of Fr (Forchheimer number). Reason behind this decrease in $f(t^*, x^*, y^*)$ is that higher Fr (Forchheimer number) being associated with more resistive force (drag forces). Such force resists hybrid nanomaterial (GO + Cu + Water) flow and hence $f(t^*, x^*, y^*)$ decreases. Figure 5 sketches impacts of M (Reynolds number) on velocity ($f(t^*, x^*, y^*)$) of hybrid nanomaterial (GO + Cu + Water). Here $f(t^*, x^*, y^*)$ intensifies with higher M (Reynolds number). In fact an intensification in $f(t^*, x^*, y^*)$ is that higher

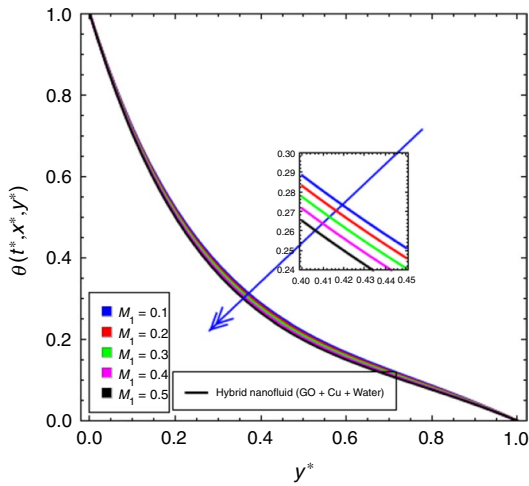


Fig. 8 Temperature $(\theta(t^*, x^*, y^*))$ against higher

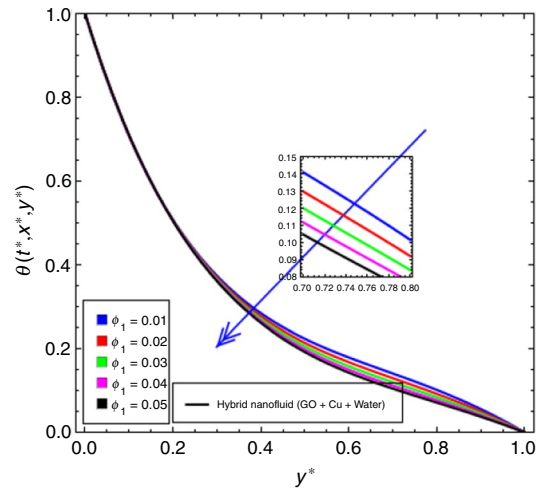


Fig. 10 Temperature $(\theta(t^*, x^*, y^*))$ against higher

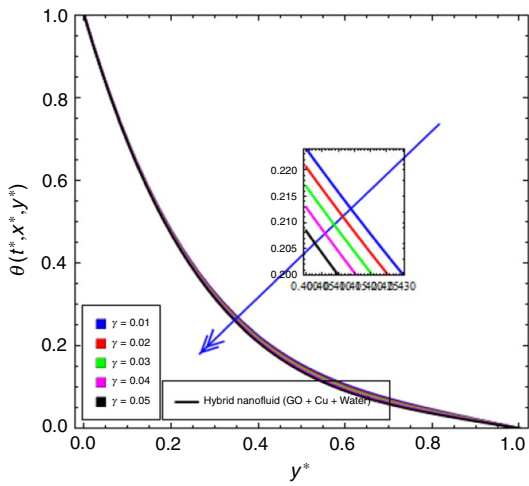


Fig. 9 Temperature $(\theta(t^*, x^*, y^*))$ against higher

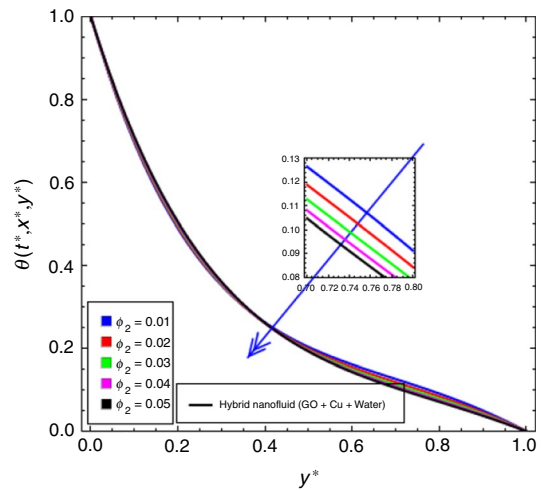


Fig. 11 Temperature $(\theta(t^*, x^*, y^*))$ against higher

M (Reynolds number) related with more turbulent flow of hybrid nanomaterial (GO + Cu + Water) and consequently $f(t^*, x^*, y^*)$ increases. Velocity $(g(t^*, x^*, y^*))$ under higher estimations of M (Reynolds number) and Sq (squeezing parameter) is labeled in Figs. 6 and 7. These figures reveal that $g(t^*, x^*, y^*)$ increases with higher M (Reynolds number) and Sq (squeezing parameter).

Discussion for $\theta(t^*, x^*, y^*)$

Temperature $(\theta(t^*, x^*, y^*))$ of the hybrid nanomaterial (GO + Cu + Water) due to increment in M_1 (melting parameter) is plotted in Fig. 8. It is examined in this figure that increase in M_1 (melting parameter) reduces $\theta(t^*, x^*, y^*)$. Higher M_1 (melting parameter) is associated with more convective flow from hot hybrid nanomaterial (GO + Cu + Water) toward the cold lower wall. As

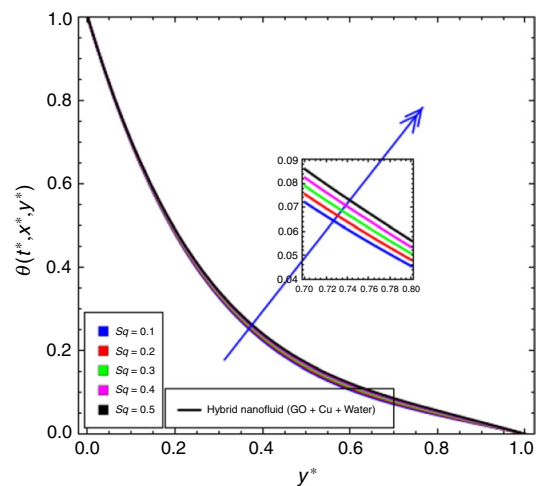


Fig. 12 Temperature $(\theta(t^*, x^*, y^*))$ against higher

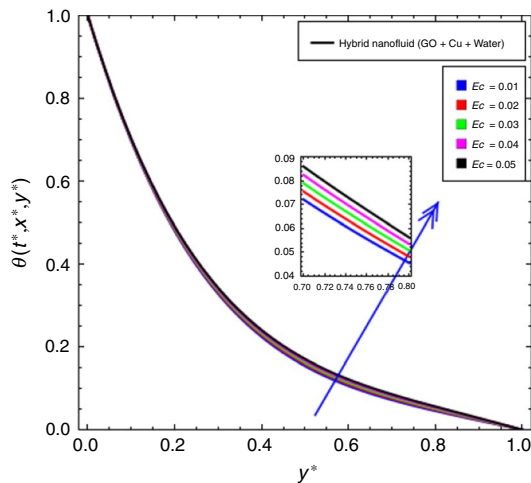


Fig. 13 Temperature $(\theta(t^*, x^*, y^*))$ against higher

a result $\theta(t^*, x^*, y^*)$ decreases. Figure 9 sketches variations in temperature $(\theta(t^*, x^*, y^*))$ for hybrid nanomaterial (GO + Cu + Water) with rise in γ (thermal relaxation parameter). This figure reveals that $\theta(t^*, x^*, y^*)$ decreases with increase in γ (thermal relaxation parameter). Figures 10 and 11 capture impacts of ϕ_1 (volume fraction for GO) and ϕ_2 (volume fraction for Cu). It is noted from these both figures that $\theta(t^*, x^*, y^*)$ declines with increase in both ϕ_1 (volume fraction for GO) and ϕ_2 (volume fraction for Cu). Reason behind this reduction is the transmission of heat form heated hybrid nanomaterial (GO + Cu + Water) toward surrounding. Hence $\theta(t^*, x^*, y^*)$ decreases. Temperature $(\theta(t^*, x^*, y^*))$ due to higher Sq (squeezing parameter) is presented in Fig. 12. It is revealed by this plot that temperature $(\theta(t^*, x^*, y^*))$ of the hybrid nanomaterial (GO + Cu + Water) increases with higher Sq (squeezing parameter). Physically higher Sq (squeezing parameter) is associated with insertion of more squeezing force from the upper wall on the hybrid nanomaterial (GO + Cu + Water). Thus, due to collision among the particles of the hybrid nanomaterial (GO + Cu + Water), more heat is generated and consequently $\theta(t^*, x^*, y^*)$ boosts. Figure 13 is plotted for studying variations in temperature $(\theta(t^*, x^*, y^*))$ due to higher Ec (Eckert number). It is observed from this plot that higher Ec (Eckert number) is directly associated with K.E (as it is the ratio of K.E and enthalpy). Hence $\theta(t^*, x^*, y^*)$ increases with Ec (Eckert number).

Final remarks

Hybrid nanomaterial (GO + Cu + Water) bounded between infinite parallel walls is examined. Melting heat and viscous dissipation elaborate heat transmission in the considered problem. Cattaneo–Christov (C–C) heat flux model is

taken into account. Worth mentioning points are that velocity (u) enlarges with an increase in (γ) (squeezing parameter) and (Re) (Reynolds number). Higher (ϕ_1) (porosity parameter) and (F) (Forchheimer number) cause decay in velocity (u) . Velocity (u) is higher for (γ) (squeezing parameter) and (Re) (Reynolds number). Higher (Ec) (Eckert number) and (γ) (squeezing parameter) intensify temperature (θ) of the fluid. Fluid temperature (θ) is controlled by choosing higher (γ) (melting parameter), (τ) (thermal relaxation time parameter), (ϕ_1) (volume fraction for GO) and (ϕ_2) (volume fraction for Cu).

Declarations

Conflict of interest It is declared that there is no conflict of interest among the authors.

References

1. Choi SUS, Eastman JA. Enhancing thermal conductivity of fluids with nanoparticles: the Proceedings of the 1995 ASME International Mechanical Engineering Congress and Exposition, San Francisco, USA, ASME, FED 231/MD, 66 (1995) 99–105.
2. Eastman JA, Choi SUS, Li S, Yu W, Thompson LJ. Anomalous increased effective thermal conductivities of ethylene glycol-based nanofluids containing copper nanoparticles. *Appl Phys Lett*. 2001;78:718–20.
3. Sarkar J, Ghosh P, Adil A. A review on hybrid nanofluids: recent research, development and applications. *Renew Sustain Energy Rev*. 2015;43:164–77.
4. Hayat T, Muhammad K, Alsaedi A, Asghar S. Numerical study for melting heat transfer and homogeneous-heterogeneous reactions in flow involving carbon nanotubes. *Results Phys*. 2018;8:415–21.
5. Hosseini SR, Ghasemian M, Sheikholeslami M, Shafee A, Li Z. Entropy analysis of nanofluid convection in a heated porous microchannel under MHD field considering solid heat generation. *Powder Technol*. 2019;344:914–25.
6. Dinarvand S, Pop I. Free-convective flow of copper/water nanofluid about a rotating down-pointing cone using Tiwari-Das nanofluid scheme. *Adv Powder Technol*. 2017;28:900–9.
7. Muhammad K, Hayat T, Alsaedi A, Asghar S. Stagnation point flow of basefluid (gasoline oil), nanomaterial (CNTs) and hybrid nanomaterial (CNTs+CuO): A comparative study. *Mater Res Express*. 2019. <https://doi.org/10.1088/2053-1591/ab356e>.
8. Eid MR, Mabood F. Entropy analysis of a hydromagnetic micropolar dusty carbon NTs-kerosene nanofluid with heat generation: Darcy–Forchheimer scheme. *J Therm Anal Calorim*. 2021;143:2419–36.
9. Ahmed F, Khan WA. Efficiency enhancement of an air-conditioner utilizing nanofluids: an experimental study. *Energy Rep*. 2021;7:575–83.
10. Nisar Z, Hayat T, Alsaedi A, Ahmad B. Wall properties and convective conditions in MHD radiative peristalsis flow of Eyring-Powell nanofluid. *J Therm Anal Calorim*. 2021;144:1199–208.
11. Souayah B, Kumar KG, Reddy MG, Rani S, Hdhiri N, Alfannakh H, Rahimi-Gorji M. Slip flow and radiative heat transfer behavior of Titanium alloy and ferromagnetic nanoparticles along with suspension of dusty fluid. *J Mol Liq*. 2019;290:111223.
12. Al-Hossainy AF, Eid MR. Combined experimental thin films, TDDFT-DFT theoretical method, and spin effect on [PEG-H₂O/

- ZrO₂+MgO/h hybrid nanofluid flow with higher chemical rate. *Surf Interfaces*. 2021;23:100971.
13. Hayat T, Ahmed B, Abbasi FM, Ahmad B. Mixed Convective Peristaltic flow of carbon nanotubes submerged in water using different thermal Conductivity Models. *Comput Methods Programs Biomed*. 2016;135:141–50.
 14. Hajizadeh A, Shah NA, Shah SIA, Animasaun IL, Rahimi-Gorji M, Alarifi IM. Free convection flow of nanofluids between two vertical plates with damped thermal flux. *J Mol Liq*. 2019;289:110964.
 15. Kahshan M, Lu D, Rahimi-Gorji M. Hydrodynamical study of flow in a permeable channel: Application to flat plate dialyzer. *Int J Hydrog Energy*. 2019;44:17041–7.
 16. Muhammad T, Lu D-C, Mahanthesh B, Eid MR, Ramzan M, Dar A. Significance of Darcy–Forchheimer porous medium in nanofluid through carbon nanotubes. *Commun Theor Phys*. 2018;70:361.
 17. Kumar KG, Avinash BS, Rahimi-Gorji M, Alarifi IM. Optical and electrical properties of Ti1-XSnXO2 nanoparticles. *J Mol Liq*. 2019;293:111556.
 18. Eid MR. Thermal characteristics of 3D nanofluid flow over a convectively heated rigid surface in a Darcy–Forchheimer porous material with linear thermal radiation: an optimal analysis. *Arab J Sci Eng*. 2020;45:9803–14.
 19. Seikh AH, Adeyeye O, Omar Z, Raza J, Rahimi-Gorji M, Alharthi N, Khan I. Enactment of implicit two-step Obrechkoff-type block method on unsteady sedimentation analysis of spherical particles in Newtonian fluid media. *J Mol Liq*. 2019;293:111416.
 20. Eid MR, Mabood F. Two-phase permeable non-Newtonian cross-nanomaterial flow with Arrhenius energy and entropy generation: Darcy–Forchheimer model. *Phys Scr*. 2020;95:105209.
 21. Hayat T, Ahmed B, Alsaedi A. Numerical investigation for peristaltic flow of Carreau-Yasuda magneto-nanofluid with modified Darcy and radiation. *J Therm Anal Calorim*. 2019;137:1168–77.
 22. Rae B, Shahraki F, Jamailahmad M, Peyghambarzadeh SM. Experimental study on the heat transfer and flow properties of γ -Al₂O₃/water nanofluid in a double-tube heat exchanger. *J Therm Anal Calorim*. 2017;127:2561–75.
 23. Turkyilmazoglu M. Single phase nanofluids in fluid mechanics and their hydrodynamic linear stability analysis. *Comput Methods Progr Biomed*. 2020;187:105171.
 24. Rashidi S, Karimi N, Mahin O, Esfahani JA. A concise review on the role of nanoparticles upon the productivity of solar desalination systems. *J Therm Anal Calorim*. 2018. <https://doi.org/10.1007/s10973-018-7500-8>.
 25. Hussain Z. Heat transfer through temperature dependent viscosity hybrid nanofluid subject to homogeneous-heterogeneous reactions and melting condition: A comparative study. *Phys Scr*. 2020;96:015210.
 26. Turkyilmazoglu M. Thermal management of parabolic pin fin subjected to a uniform oncoming airflow: optimum fin dimensions. *J Therm Anal Calorim*. 2021;143:3731–9.
 27. Alsaedi A, Nisar Z, Hayat T, Ahmad B. Analysis of mixed convection and hall current for MHD peristaltic transport of nanofluid with compliant wall. *Int Commun Heat Mass Transfer*. 2021;121:105121.
 28. Turkyilmazoglu M. Nanoliquid film flow due to a moving substrate and heat transfer. *Eur Phys J Plus*. 2020;135:781.
 29. Roberts L. On the melting of a semi-infinite body of ice placed in a hot stream of air. *J Fluid Mech*. 1958;4:505–28.
 30. Qayyum S, Khan R, Habib H. Simultaneous effects of melting heat transfer and inclined magnetic field flow of tangent hyperbolic fluid over a nonlinear stretching surface with homogeneous–heterogeneous reactions. *Int J Mech Sci*. 2017;133:1–10.
 31. Qi R, Wang Z, Ren J, Wu Y. Numerical investigation on heat transfer characteristics during melting of lauric acid in a slender rectangular cavity with flow boundary condition. *Int J Heat Mass Transfer*. 2020;157:119927.
 32. Ho CJ, Gao JY. An experimental study on melting heat transfer of paraffin dispersed with AlO nanoparticles in a vertical enclosure. *Int J Heat Mass Transfer*. 2013;62:2–8.
 33. Das K. Radiation and melting effects on MHD boundary layer flow over a moving surface. *Ain Shams Eng J*. 2014;5:1207–14.
 34. Hayat T, Muhammad K, Alsaedi A. Melting effect in MHD stagnation point flow of Jeffrey nanomaterial. *Phys Scr*. 2019. <https://doi.org/10.1088/1402-4896/ab210e>.
 35. Motahar S. Experimental study and ANN-based prediction of melting heat transfer in a uniform heat flux PCM enclosure. *J Energy*. 2020;30:101535.
 36. Hayat T, Muhammad K, Alsaedi A, Ahmad B. Melting effect in squeezing flow of third-grade fluid with non-Fourier heat flux model. *Phys Scr*. 2019. <https://doi.org/10.1088/1402-4896/ab1c2c>.
 37. Ibrahim W. Magnetohydrodynamic (MHD) boundary layer stagnation point flow and heat transfer of a nanofluid past a stretching sheet with melting. *Propuls Power Res*. 2017;6:214–22.
 38. Hayat T, Muhammad K, Alsaedi A, Asghar S. Thermodynamics by melting in flow of an Oldroyd-B material. *J Braz Soc Mech Sci Eng*. 2018;40:530.
 39. Khan MdS, Alam M, Tzirtzilakis E, Ferdows M. Finite difference simulation of MHD radiative flow of a nanofluid past a stretching sheet with stability analysis. *Int J Adv Thermofluid Res*. 2016;2:15–30.
 40. Ahmad S, Hayat T, Alsaedi A. Numerical analysis of entropy generation in viscous nanofluid stretched flow. *Int Commun Heat Mass Transfer*. 2020;117:104772.
 41. Bisht A, Sharma R. Non-similar solution of Sisko nanofluid flow with variable thermal conductivity: a finite difference approach. *Int J Numer Meth Heat Fluid Flow*. 2020;31:345–66.
 42. Davydov O, Safarpoor M. A meshless finite difference method for elliptic interface problems based on pivoted QR decomposition. *Appl Numer Math*. 2021;161:489–509.
 43. Benito JJ, García A, Gavete L, Negreanu M, Ureña F, Vargas AM. Solving Monge–Ampère equation in 2D and 3D by generalized finite difference method. *Eng Anal Bound Elem*. 2021;124:52–63.

Publisher's Note Springer Nature remains neutral with regard to jurisdictional claims in published maps and institutional affiliations.